Postzygotic barriers persist despite ongoing introgression in hybridizing *Mimulus* species

Samuel J. Mantel[1*] and Andrea L. Sweigart[1]

[1]Department of Genetics, University of Georgia, Athens, GA, 30602, USA

[*]Corresponding author:
Samuel Mantel
120 E. Green St.
Athens, GA 30602
smantel1@uga.edu

Word Count: 6471
- Introduction: 987
- Materials and Methods: 1959
- Results: 1603
- Discussion: 1922

Number of Figures: 4
Number of Color Figures: 3
Number of Tables: 3
Number of Supplemental Figures: 18
Number of Supplemental Tables: 5

Summary

- The evolution of postzygotic isolation is thought to be a key step in maintaining species boundaries upon secondary contact, yet the dynamics and persistence of hybrid incompatibilities in sympatric species are not well understood.
- Here, we explore these issues using genetic mapping in three populations of recombinant inbred lines between naturally hybridizing monkeyflowers *Mimulus guttatus* and *M. nasutus* from the sympatric Catherine Creek population.
- The three *M. guttatus* founders differ dramatically in admixture history. Comparative genetic mapping also reveals three putative inversions segregating among the *M. guttatus* founders, two due to admixture. We observe strong, genome-wide transmission ratio distortion, but patterns are highly variable among populations. Some distortion is explained by epistatic selection favoring parental genotypes, but tests of inter-chromosomal linkage disequilibrium also reveal multiple candidate Dobzhansky-Muller incompatibilities. We also map several genetic loci for hybrid fertility, including two interacting pairs coinciding with peaks of distortion.
- Remarkably, in this limited sample of *M. guttatus*, we discover abundant segregating variation for hybrid incompatibilities with *M. nasutus,* suggesting this population harbors diverse contributors to postzygotic isolation. Moreover, even with substantial admixture, hybrid incompatibilities between *Mimulus* species persist, suggesting postzygotic isolation might be a potent force in maintaining species barriers in this system.

Key Words: Introgression; transmission ratio distortion; hybrid Incompatibility; sterility; reproductive isolation; *Mimulus*

Introduction

Despite often being conceptualized as a single event, it has long been understood that speciation is a complex and dynamic process (Darwin, 1859; Dobzhansky, 1937). As new species form (generally in allopatry), the cumulative impacts of adaptive divergence, genetic drift, and the sorting of ancestral variation can lead to the evolution of reproductive isolation, which limits gene flow between species when they come into secondary contact (Dobzhansky, 1937; Mayr, 1942; Coyne & Orr, 2004). Nevertheless, gene flow between recognized species – at rates high enough to have substantial genomic consequences – is not uncommon, even when strong reproductive isolating barriers exist (Nolte *et al.*, 2009; Teeter *et al.*, 2010; Ellegren *et al.*, 2012; Renaut *et al.*, 2013; Larson *et al.*, 2014; Delmore *et al.*, 2015; Caeiro-Dias *et al.*, 2023). At the extremes, hybridization can break down established barriers causing previously isolated lineages to fuse (Taylor *et al.*, 2006) or strengthen reproductive isolation through reinforcement (Servedio & Kirkpatrick, 1997; Jaenike et al., 2006; Hopkins & Rausher, 2012), but theory also suggests partial reproductive isolation can sometimes evolve as a stable optimum (Servedio & Hermisson, 2020). Studies of naturally hybridizing species can provide a window into the causes of these alternative evolutionary outcomes, allowing us to identify and measure the impact of the genetic loci involved in reproductive isolation.

One powerful approach to address these questions is experimental hybridization of incompletely isolated species that occur together in secondary sympatry. In particular, the use of late-generation hybrids such as recombinant inbred lines (RILs) can enable replication of wild, admixed genotypes and facilitate genetic mapping of barrier loci under controlled, environmental conditions. This approach should be especially fruitful for identifying loci

71 involved in postzygotic isolation because strongly incompatible allele combinations are likely to
72 be purged during RIL formation. Indeed, selection against hybrid incompatibilities can be a
73 major source of transmission ratio distortion (TRD) in RIL populations (Colomé-Tatché &
74 Johannes, 2016). Although there are often additional contributors to TRD in experimental
75 hybrid populations (reviewed in Fishman & McIntosh, 2019), hybrid incompatibilities are
76 expected to leave a particular signature of distortion, generating both local peaks and linkage
77 disequilibrium between unlinked loci caused by underrepresented or absent multi-locus
78 genotypes. This signature will likely be particularly apparent in RILs, which have the advantage
79 of multiple generations of recombination, increasing power to detect and localize
80 incompatibilities by amplifying their effects (and revealing recessive phenotypes) through
81 inbreeding (Moyle & Nakazato, 2008).

82 Despite the clear value of experimental hybridization, and RILs in particular, for
83 illuminating the genetic causes of reproductive isolation, inferences to natural populations can
84 be challenging because such studies are often based on crosses between only two individuals or
85 inbred lines. This limitation might be serious for investigations of postzygotic isolation between
86 species in the early stages of divergence, as hybrid incompatibilities are often polymorphic
87 (Sweigart *et al.*, 2007; Good *et al.*, 2008; Cutter, 2012), particularly in populations with ongoing
88 hybridization (Zuellig & Sweigart, 2018a). Variation in chromosomal structure is also a common
89 feature of natural populations (Hoffmann & Rieseberg, 2008), and polymorphic inversions are
90 often associated with adaptive differences (Feder *et al.*, 2003; Lowry & Willis, 2010; Jones *et al.*,
91 2012) and reproductive isolation (Noor *et al.*, 2001b; Sotola *et al.*, 2023). One way to capture a
92 more representative set of natural variation is to generate a multi-parent mapping population,

93 for instance by performing multiple biparental crosses to a common founder (Yu *et al.*, 2008).
94 Although this strategy is now routinely used in plant breeding programs (Scott *et al.*, 2020) and
95 to dissect the genetics of complex traits (Aylor *et al.*, 2011; Long *et al.*, 2014) it has rarely been
96 applied to studies of speciation.

97 In this study we investigate patterns and mechanisms of reproductive isolation in three
98 independent RIL populations constructed from crosses between *Mimulus guttatus* and *M.*
99 *nasutus* (also referred to as *Erythranthe guttata* and *E. nasuta*: see Lowry *et al.*, 2019 and
100 Nesom *et al.*, 2019). These two species are closely related (~200 KYA diverged: Brandvain *et al.*,
101 2014), and broadly allopatric across western North America, but occur in secondary sympatry at
102 many sites in their shared range. One such sympatric site occurs at Catherine Creek (CAC) in
103 Washington state, a system of ephemeral seeps and streams that flow into the Columbia River.
104 These *Mimulus* species have diverged in mating system (*M. guttatus* is large flowered and
105 predominantly outcrossing, whereas *M. nasutus* is a small flowered and primarily selfing), which
106 acts as a strong premating barrier where the two species co-occur (Martin & Willis, 2007). At
107 Catherine Creek, divergent flowering phenology (Fishman *et al.*, 2014a; Kenney & Sweigart,
108 2016) and microhabitat adaptation (Mantel & Sweigart, 2019) are also important contributors
109 to premating isolation. Despite these substantial barriers to interspecific mating, studies of
110 population genomic variation at Catherine Creek have revealed clear signatures of historical and
111 contemporary hybridization (Kenney & Sweigart, 2016), resulting in largely unidirectional
112 introgression from *M. nasutus* into *M. guttatus* (Sweigart & Willis, 2003; Brandvain *et al.*, 2014;
113 Kenney & Sweigart, 2016). Even in the absence of interspecific gene flow, *M. guttatus*

114 populations are exceptionally genetically diverse (Flagel *et al.*, 2014; Puzey *et al.*, 2017) and
115 maintain substantial variation for complex phenotypes (Troth et al., 2018).
116 Here, we attempt to capture and leverage this diversity at Catherine Creek to
117 understand the patterns and mechanisms of hybrid breakdown in naturally hybridizing species.
118 We generate three independent RIL populations by crossing distinct CAC *M. guttatus*
119 progenitors to a common *M. nasutus* parent. Using this powerful crossing design, we discover
120 that differences in admixture have cascading effects on structural variation and reproductive
121 barriers. Moreover, even in this small sample of three *M. guttatus* lines, we find segregating
122 variation for hybrid incompatibilities with *M. nasutus*, suggesting this population harbors
123 diverse contributors to postzygotic isolation. Finally, we discover that even with substantial
124 admixture, hybrid incompatibilities between *Mimulus* species persist, suggesting postzygotic
125 isolation might be a potent force in maintaining species barriers in the face of ongoing
126 hybridization.

127 **Materials and Methods**

128 *Plant Material and Crossing Design*

129 The plants used in this study are derived from a collection of inbred lines (>10
130 generations inbred, single seed decent) produced from wild-collected seeds from Catherine
131 Creek (CAC). We produced three parallel RIL populations from crosses between these inbred
132 lines of CAC *M. guttatus* and *M. nasutus*. We selected three previously studied CAC *M. guttatus*
133 inbred lines (CAC110, CAC162, and CAC415; TableS1; Mantel & Sweigart, 2019) with stereotypic
134 *M. guttatus* morphological and phenological characteristics and which produced fertile F1s with
135 *M. nasutus* (~72-99% viable pollen). One *M. nasutus* inbred line (CAC9) served as a common
136 maternal parent, which we emasculated before pollen development, and crossed by hand with
137 pollen from each of the *M guttatus* inbred lines, producing three F1 hybrids. For each of these
138 F1 hybrids, we self-fertilized a single plant to generate three corresponding F2 populations (*N* =
139 500 plants each). We performed several additional rounds of self-fertilization using single-seed-
140 descent to produce three populations of F6 or F7 recombinant inbred lines (RILs; Figure S1),
141 generating a total of 368 RILs (151 CAC110 RILs, 128 CAC162 RILs, and 89 CAC415 RILs), much
142 lower than the initial 1500 due to line extinction during the inbreeding process.

143

144 *Library Preparation, Sequencing, and Processing*

145 We grew one individual of each of the 368 RILs (F6 generation or later) for tissue
146 collection and DNA extraction in the greenhouse at the University of Georgia, conditions
147 described in Supporting Information Methods S1. We collected bud and meristem tissue from
148 each individual into 96-well plates on dry ice, stored them at -80°C, and extracted genomic DNA

149 using a modified CTAB method in a 96-well format

150 (dx.doi.org/10.17504/protocols.io.bgv6jw9e). We then constructed ddRADseq libraries using a

151 modified version of RAD Capture (Ali *et al.*, 2016), "BestRAD"

152 (dx.doi.org/10.17504/protocols.io.6awhafe, Supporting Information Methods S1). We prepared

153 libraries for, and sequenced the same RILs twice, each on two partial lanes of Illumina

154 HiSeq4000 for paired end 150-bp reads at the Genome Sequencing Facility at Duke University.

155 We also extracted genomic DNA from bud and leaf tissue of the three parental CAC *M. guttatus*

156 lines using a modified CTAB method as above. Whole genome sequence (WGS) libraries were

157 prepared and sequenced on a partial lane of Illumina HiSeq4000 for paired end 150-bp reads at

158 the Genome Sequencing Facility at Duke University.

159 We aligned WGS reads to the *Mimulus guttatus* IM62 v3 refence assembly

160 (phytozome.org, IM: Iron Mountain, an allopatric *M. guttatus* population in Oregon, ~200km

161 south of CAC), called SNPs, removed heterozygous calls and filtered sites to a minimum depth of

162 3x, and a maximum depth of 2 standard deviations above the mean. To aid in genotyping *M.*

163 *guttatus* and *M. nasutus* SNPs across the genome, we identified a full list of diagnostic SNPs

164 (i.e., those homozygous for different alleles in each of the parental pairs, CAC9 & CAC110, CAC9

165 & CAC162, and CAC9 & CAC415). We joint genotyped each pair of parental lines, quality filtered

166 the called SNPs, and retained only biallelic SNPs, extracting a list of high-quality, diagnostic SNPs

167 for each pair of parental lines. Details of sequence data processing are described in Supporting

168 Information Methods S1.

169 Following sequencing, we demultiplexed the ddRADseq data and aligned reads to the

170 *Mimulus guttatus* IM62 v3 reference assembly. At this stage, six samples were removed from

171 further analysis (4 from the CAC162 RILs, and 2 from the CAC415 RILs) due to low similarity
172 between duplicate BAMs produced from the two independent ddRAD library preparations. We
173 then merged the remaining duplicate BAMs for a total of 362 RIL individuals (151 CAC110 RILs,
174 124 CAC162 RILs, and 87 CAC415 RILs). We called SNPs, joint genotyped each RIL population
175 with its corresponding parental lines, and quality filtered called SNPs. Finally, we removed non-
176 diagnostic sites between each pair of parental lines.
177 To assess levels of residual heterozygosity in the RIL populations, we filtered the three
178 RIL VCFs as above and requiring a minimum depth of 10x. Heterozygosity was low and uniform
179 across the genome: CAC110 RILs: 1.95%, N=13,975; CAC162 RILs: 2.34%, N=33,340; CAC415
180 RILs: 2.79%, N=23,178 and consistent with the Mendelian expectation (~1.5-3%, in F6/F7 RILs).
181
182 *Assessment of Introgression in Parental Lines*
183 As previous studies have shown that admixture between *M. guttatus* and *M. nasutus* is
184 common at CAC (Brandvain *et al.*, 2014; Kenney & Sweigart, 2016) we first checked the selected
185 CAC *M. guttatus* parental lines for evidence of introgression from *M. nasutus*. To coarsely
186 identify putative regions of introgression in *M. guttatus* parental lines, we calculated *Dxy*
187 between CAC9 and the three parental *M. guttatus* lines in non-overlapping 50-kb windows
188 containing 5000 or more called sites. To more concretely assess evidence of *M. nasutus*
189 introgression in the parental CAC *M. guttatus* lines, we used the newly generated WGS data,
190 plus WGS data from 7 other inbred *Mimulus* accessions downloaded from the SRA
191 (https://www.ncbi.nlm.nih.gov/sra, Table S1): the parental *M. nasutus* line CAC9, 3 non-CAC *M.*
192 *nasutus* lines, the 3 parental *M. guttatus* lines from CAC, 5 additional non-parental *M. guttatus*

193 lines from CAC, and 2 non-CAC *M. guttatus* lines). We processed reads from additional (non-
194 parental) lines as above and joint genotyped all lines together. We filtered called SNPs based on
195 quality as above, and retained only biallelic SNPs.

196 We identified putative regions of introgression using a Hidden Markov Model (HMM,
197 modified from Durbin *et al.*, 1998 and developed in Brandvain *et al.*, 2014. As an input for the
198 model, we identified fourfold degenerate sites and non-degenerate sites in the IM62 v3
199 reference assembly (https://github.com/tsackton/linked-selection/tree/master/misc_scripts).
200 With these lists and the VCF of high-quality filtered SNPs in parental and non-parental *Mimulus*
201 lines described above, we counted the total number of genotyped sites, genotyped non-
202 degenerate sites, and genotyped fourfold degenerate sites in 1-kb windows in each line. We
203 then counted the number of those sites that differed in their SNP call between each pairwise
204 comparison of lines. With these counts and the HMM, we calculated posterior probabilities of
205 *M. nasutus* and *M. guttatus* ancestry across the genomes of the parental CAC *M. guttatus* lines.
206 We considered 1-kb windows with a calculated posterior probability of *M. nasutus* ancestry
207 >0.95 to be windows showing evidence of introgression.

208

209 *RIL Genotyping and Linkage Mapping*

210 We genotyped the RILs in non-overlapping 50-kb windows; windows with >75% *M.*
211 *guttatus* calls were coded as *M. guttatus* homozygotes, 25-75% as heterozygotes, and <25% as
212 M. nasutus homozygotes. Windows with no SNP calls were coded as missing data. To fill these
213 gaps, we used Python scripts from the processing steps of the program GOOGA (Flagel *et al.*,
214 2019) to calculate genotype probabilities for each window in each RIL individual. In GOOGA, we

215 set the expected genotype frequencies to 1:1 for alternative parental homozygotes
216 (heterozygotes are excluded given that they are <3% of the genotypes in this advanced RIL
217 population). We then used the program to estimate genotype error rates and recombination
218 rates for each windowed genotype for each RIL. We dropped 39 RILs from the dataset due to
219 excessive missing data (stemming from low read coverage) because they produced high (e1 or
220 e2 > 0.2) estimated error rates in GOOGA (8 from the CAC110 RILs, 26 from the CAC162 RILs,
221 and 5 from the CAC415 RILs). Finally, we used GOOGA's HMM to estimate genotype
222 probabilities for each 50-kb window of the remaining RILs and converted to hard calls excluding
223 windows with probabilities <0.75. Of the original 368 RILs, this resulted in genotype data for 323
224 of them (143 of the original 151 from the CAC110 RILs, 98/128 from the CAC162 RILs, and 82/89
225 from the CAC415 RILs). We used LepMAP3 (Rastas, 2017) to construct a linkage map for each of
226 the three RIL populations. Linkage mapping details are described in Supporting Information
227 Methods S1 and Table S2. We produced three linkage maps containing 3,828, 4,389 and 4,379
228 markers, retaining 794, 606, and 690 that mapped to recombination-informative sites (for the
229 CAC110, CAC162, and CAC415 RIL populations, respectively).
230
231 *Assessment of Transmission Ratio Distortion and Linkage Disequilibrium*
232 Following linkage mapping, we calculated genotype frequencies at each marker in each
233 map and identified regions of transmission ratio distortion (TRD) by testing for deviations from
234 the Mendelian 1:1 expectation with χ^2 tests. We used both an uncorrected $\alpha = 0.01$ and a more
235 stringent Bonferonni-corrected α (unique α for each chromosome in each RIL population
236 depending on the number of markers tested; Table S3). To investigate whether peaks of TRD

237 were associated with major two-locus hybrid incompatibilities we used the package pegas
238 (Paradis, 2010) to characterize pairwise linkage disequilibrium (LD) between all markers with
239 unique map positions. To minimize false positives driven by the large number of pairwise
240 comparisons, we identified putative interacting loci associated with inter-chromosomal LD
241 based on r values greater than the 95% percentile (CAC110 RILs: $r > 0.37$, CAC162 RILs: $r > 0.41$,
242 CAC415 RILs: $r > 0.39$). At these interacting loci we then performed likelihood ratio tests
243 comparing observed genotype ratios to expected ratios (calculated by cross tabulation of
244 observed allele frequencies), and describe epistatic interactions where $p<0.0001$.
245
246 *Assessment of Hybrid Male and Female Sterility*
247 To measure male fertility, we collected pollen from three flowers (second flower pair or
248 later) of each RIL individual. We suspended the pollen of each flower separately in lactophenol-
249 aniline blue stain (Kearns & Inouye, 1993) and inspected the pollen grains using a compound
250 microscope. For each flower, we estimated pollen fertility by calculating the proportion of darkly
251 stained (viable) pollen grains from a haphazardly selected group of >100 within a field of view in
252 of the microscope. When fertility estimates from flowers of the same plant differed by more
253 than 0.2, pollen from up to three more flowers was collected and counted. We then estimated
254 individual pollen viability as the average value from all collected flowers. Because the
255 distribution of pollen viability in each RIL population was left-skewed, we logit-transformed the
256 data to more closely match a normal distribution.
257 To estimate hybrid female sterility, we intercrossed random pairs of RILs in at least
258 duplicate, and collected all seeds produced. We counted the number of seeds produced per

259 fruit for each cross made and ran a linear mixed model (LMM, using the lmer command in the
260 'lme4' package). In addition to maternal parent genotype (fixed effect), the model included
261 average viable pollen proportion of the paternal parent (as calculated above, fixed effect), a
262 unique RIX identifier nested within RIX cross type (CAC110 RIL x CAC162 RIL, CAC162 RIL x
263 CAC415 RIL, etc.; random effect) and the year that the cross was made (crosses were made
264 during two separate grow-outs in separate years; random effect). We then calculated least
265 square means of female fertility (using seeds per fruit as a proxy) for each RIL genotype using
266 the 'emmeans' package. This method produced distributions with a long right tail, so we square
267 root transformed the data to more closely match a normal distribution.
268
269 *QTL Mapping*
270 Given the small sample sizes of each RIL population, we took a multistep approach to
271 genetically map hybrid male and female sterility. For each trait in each RIL population, we first
272 used r/QTL (Broman & Sen, 2009; Arends *et al.*, 2010) to perform 10 iterations of composite
273 interval mapping (CIM; Zeng, 1993, 1994; Jansen & Stam, 1994). Because CIM requires no
274 missing data, missing genotypes are imputed before the scan is run, leading to potential
275 differences among iterations. We set lenient LOD thresholds ($\alpha = 0.15$) for QTL significance, by
276 performing 5,000 permutations, and calculated 1.5-LOD intervals ('lodint' command) for each
277 significant peak position in any of the 10 iterations. We then performed single-QTL scans using
278 each QTL identified with CIM as an interactive covariate ('intcovar' option) in separate runs. We
279 again we set LOD thresholds ($\alpha = 0.15$, 10,000 permutations) for interacting QTL significance,
280 and calculated 1.5-LOD intervals for each significant peak position. With these identified peaks,

281 we then fit a multiple-QTL model ('fitqtl' command; HK method) and directly estimated additive

282 QTL effects (at each peak position) and identified epistatic effects. We then removed any

283 nonsignificant ($p > 0.05$) effects, and re-fit the model.

Results

Admixture in M. guttatus parental lines

All *M. guttatus* lines tested show clear evidence of admixture from *M. nasutus*, but the genomic location and proportion of introgression vary considerably across lines (Figure 1, Figure S2, Figure S3). Of the three parents, CAC110 is the most admixed with ~24% of its genome showing very low genetic divergence (*Dxy*) and a high posterior probability of recent coalescence with *M. nasutus* via probabilistic inference (HMM, see Methods; Brandvain *et al.*, 2014). At least some of this introgression in CAC110 appears to be recent, with large portions of entire chromosome arms showing evidence of introgression (Figure S2). Although the largest inferred contiguous blocks in CAC110 are only ~1.1Mb (Figure S4b), the HMM may sometimes break up true contiguous blocks of introgression (or incorrectly identify short regions with low *Dxy* as admixture blocks – see Brandvain et al. 2014). Given the improbability of inheriting a large number of small introgressions immediately adjacent to one another, we think it likely that several regions in CAC110 (on Chromosomes 1, 8, 11, and 13 – Figure 1 and Figure S2) represent true contiguous blocks of admixture. In both CAC162 and CAC415, the overall proportion of admixture is lower (~9% in each) and blocks are generally smaller and more evenly dispersed throughout the genome (Figure S2; Figure S4b), consistent with introgression events that occurred in the more distant past. Even in CAC110, however, there are many very small regions of inferred introgression (Figure S4b), suggesting *M. guttatus* genomes at Catherine Creek are shaped by a long history of introgression from *M. nasutus*.

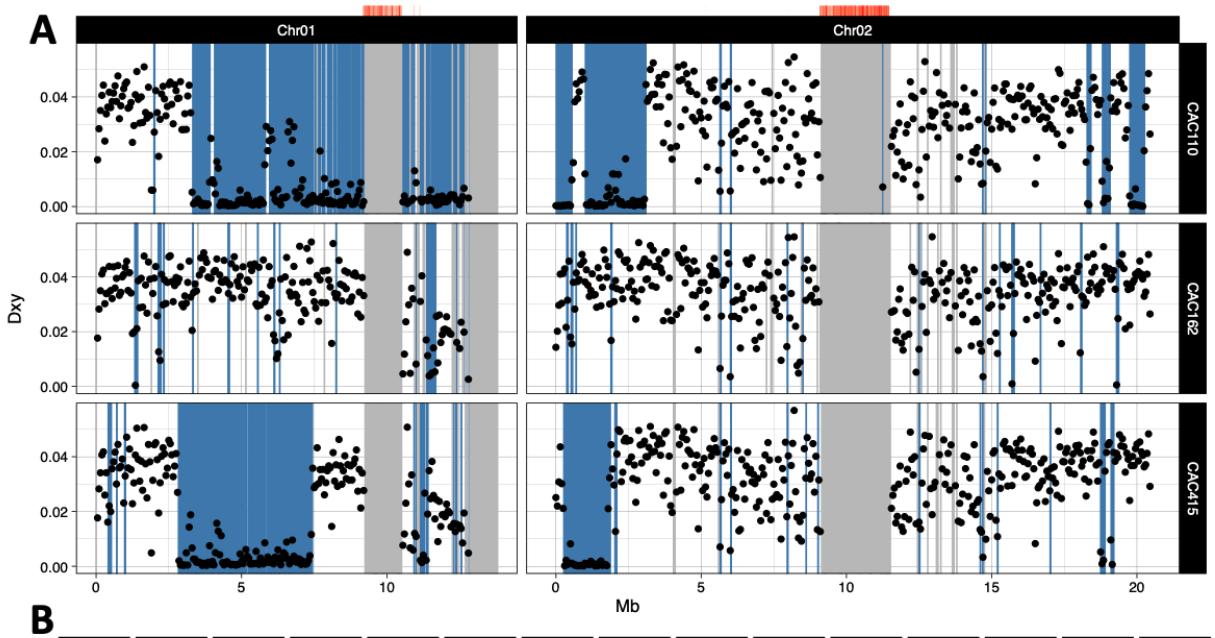

B

	Chr01	Chr02	Chr03	Chr04	Chr05	Chr06	Chr07	Chr08	Chr09	Chr10	Chr11	Chr12	Chr13	Chr14	Genome
CAC110	46.18%	18.90%	11.93%	32.88%	14.65%	5.31%	7.92%	32.65%	14.82%	17.93%	54.44%	15.10%	40.03%	10.13%	23.83%
CAC162	4.68%	3.25%	6.33%	8.73%	6.41%	13.48%	23.40%	18.54%	6.07%	12.56%	9.89%	4.78%	1.94%	9.15%	9.24%
CAC415	32.17%	10.67%	11.46%	8.78%	5.86%	8.15%	9.72%	4.82%	5.03%	8.55%	14.22%	7.05%	2.54%	2.94%	8.61%

Figure 1. Introgression from *M. nasutus* into sympatric *M. guttatus*. (a) *Dxy* calculated in 50kb windows across the first two chromosomes of the IM62 v3 *Mimulus guttatus* reference genome, between the parental lines of the three RIL populations (CAC9 v. CAC110, CAC9 v. CAC162, and CAC9 v. CAC415). Blue shaded regions indicate putatively admixed regions in the three focal CAC *M. guttatus* lines tested, diagnosed by a greater than a 95% posterior probability of *M. nasutus* ancestry (in 1kb windows) as inferred via the HMM (i.e. more recent coalescence with included *M. nasutus* samples than with included *M. guttatus* samples). Grey shaded regions indicate missing data (fewer than 5000 genotyped sites within any 50kb window). Red heatmaps above each chromosome indicate the density of centromeric repeats in the same 50kb windows. All chromosomes are shown in Figure S2. **(b)** Heatmap showing the proportion of *M. nasutus* ancestry in each chromosome, and across the genome, of each of the three CAC *M. guttatus* lines used as parents of the RIL populations, as estimated as the proportion of 1kb windows with a greater than a 95% posterior probability of *M. nasutus* ancestry as inferred via the HMM. Darker blue shading indicates a higher proportion of *M. nasutus* ancestry.

319 *Comparative linkage mapping*

320 Across most of the genome, the three RIL linkage maps are colinear with similar lengths
321 (Table 1), and marker order generally follows the physical order of the *M. guttatus* IM62 v3
322 reference assembly (Figure 2; Figure S5). However, we identified three clear exceptions to this
323 pattern, where maps differ due to parental variation in putative inversions, characterized by a
324 large number of physically dispersed markers mapping to the same genetic position. Two of
325 these putative inversions are on LG1 (*inv1.1* and *inv1.2;* Figure S6) and are potentially unique to
326 Catherine Creek (or locally distributed), having not been reported in other crosses with these
327 *Mimulus* species (Fishman *et al.*, 2014b; Flagel *et al.*, 2019). In both cases, the CAC9 *M. nasutus*
328 parent carries the ancestral orientation and the *M. guttatus* parents segregate for the derived
329 variant. At *inv1.1*, recombination is suppressed in the CAC110 and CAC415 RILs, but not in the
330 CAC162 RIL, indicating collinearity between the CAC9 *M. nasutus* and CAC162 *M. guttatus*
331 parents (Figure 2; Figure S6). At *inv1.2*, on the other hand, the genetic maps suggest CAC9 is
332 collinear only with CAC110 (Figure 2; Figure S6). Remarkably, this *M. guttatus* parent also carries
333 a large block of introgression spanning this entire region (Figure 1), suggesting that gene flow
334 from *M. nasutus* has re-introduced the ancestral variant into CAC110. We discovered a similar
335 situation on LG13, where introgression from *M. nasutus* accounts for collinearity between CAC9
336 and CAC110 at *inv13* (recombination rates in the CAC110 RIL are much higher in this region than
337 in the CAC162 and CAC415 RILs; Figure S5). Additionally, *inv13* might have arisen in *M. nasutus*,
338 as it also appears to be present in the reference genome assembly of *M. nasutus* SF5 (an
339 accession derived from Shear's Falls, an allopatric *M. nasutus* population ~70 km from CAC), but
340 not in other recently assembled *M. guttatus* genomes (phytozome.org). Taken together, these

341 **Table 1. Summary of linkage map length and intrascaffold recombination rate estimates.** Total
342 map length and intrascaffold recombination rate estimates for each chromosome, plus total
343 map length and average recombination rate in each of the three RIL populations.

		CAC110 RILs		CAC162 RILs		CAC415 RILs	
Chromosome	Reference Length (Mb)	Map Length (cM)	cM/Mb	Map Length (cM)	cM/Mb	Map Length (cM)	cM/Mb
1	13.88	134.368	9.68	66.451	4.79	74.470	5.37
2	20.54	86.970	4.23	79.725	3.88	85.500	4.16
3	23.80	82.263	3.46	64.360	2.70	67.161	2.82
4	22.81	82.362	3.61	84.446	3.70	92.822	4.07
5	21.77	90.440	4.15	82.863	3.81	92.963	4.27
6	20.89	99.115	4.74	95.776	4.58	104.195	4.99
7	21.88	72.643	3.32	60.311	2.76	89.304	4.08
8	27.69	109.184	3.94	117.963	4.26	117.700	4.25
9	25.15	63.801	2.54	92.286	3.67	98.934	3.93
10	22.12	89.656	4.05	106.661	4.82	104.910	4.74
11	33.60	137.499	4.09	88.907	2.65	91.633	2.73
12	25.84	101.548	3.93	82.763	3.20	81.868	3.17
13	30.77	117.730	3.83	78.866	2.56	105.060	3.41
14	28.29	134.029	4.74	109.580	3.87	128.236	4.53
Global	339.04	1401.608	4.13	1210.958	3.57	1334.756	3.94

344

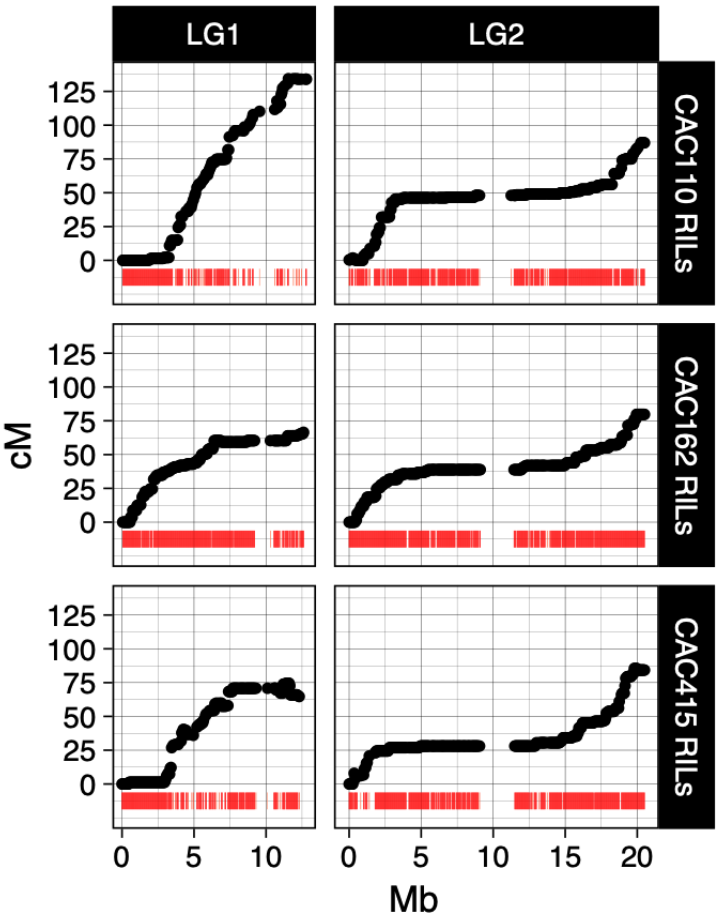

Figure 2. Map position (cM) versus physical marker positions (Mb) for the first two chromosomes of the IM62 v3 *Mimulus guttatus* reference genome in the three RIL populations. Red heatmaps below each curve indicate the density of markers, measured as the distance in Mb to the nearest neighboring marker. Low SNP density, and the subsequent inability to genotype markers in areas of the *M. guttatus* parental genomes showing evidence of introgression from *M. nasutus,* manifests as regions of low marker density on some chromosomes. All linkage groups are shown in Figure S5.

353 mapping results point to introgression from *M. nasutus* as a major source of large-scale
354 structural variation at Catherine Creek, responsible both for restoring ancestral variants and for
355 introducing new derived inversions into *M. guttatus*.
356 In addition to the effects of structural variation, we observed some instances of map
357 length variation that appear to be associated only with parental differences in introgression. In
358 the CAC110 RILs, introgressed regions on LGs 1, 11, 12, and 13 have elevated genetic distances
359 relative to the same (non-introgressed) regions in the other two RIL populations (Table 1, Figure
360 2, Figure S5). Rather than reflecting a biological difference in recombination frequency between
361 introgressed and non-introgressed regions, we attribute this effect to technical differences
362 arising from the much lower marker densities in introgressed regions, which are highly similar
363 to the CAC9 parent (Table 1, Figure 2, Figure S5).
364
365 *Genome-wide patterns of transmission ratio distortion (TRD)*
366 With the exception of LG9, we observed strong TRD in at least one RIL population on all
367 linkage groups (Figure 3, Figure S7, Table S3). Globally, patterns of TRD are highly variable across
368 RIL populations. In the CAC110 and CAC415 RILs, the majority of distorted markers show an
369 excess of *M. guttatus* genotypes (~59% in CAC110 and ~80% in CAC415), whereas in the CAC162
370 RILs, there is a strong deficit of *M. guttatus* across the genome (~89% of distorted markers show
371 an excess of *M. nasutus*). In a few cases, the same region is even distorted in opposite directions
372 (e.g., at the beginning of LG4: *M. guttatus* excess in CAC110 RILs, *M. nasutus* excess in CAC162
373 RILs; Figure 3, Figure S7). Despite this general variability, there are a few instances of shared
374 distortion in multiple RIL populations, potentially implying the same causal mechanisms. Most

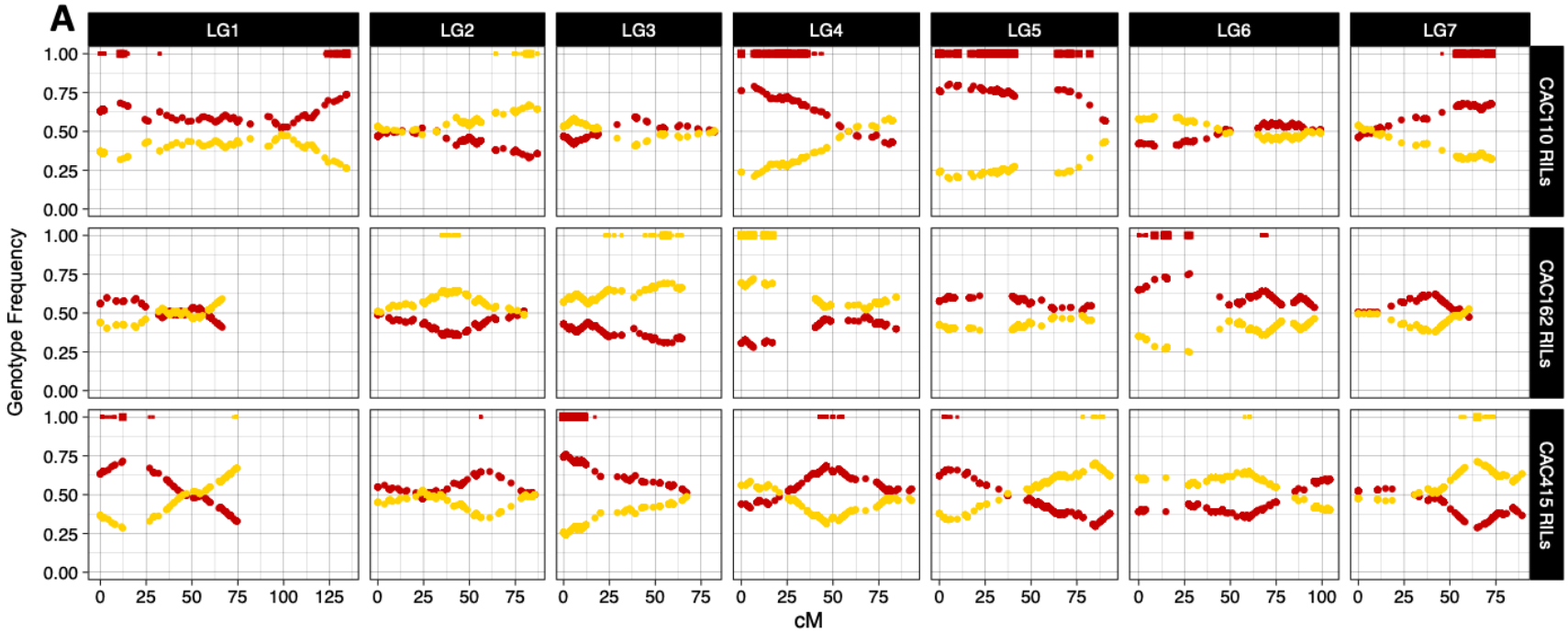
A
LG1
LG2
LG3
LG4
LG5
LG6
LG7
CAC110 RILs
CAC162 RILs
CAC415 RILs
Genotype Frequency
1.00
0.75
0.50
0.25
0.00
0
25
50
75
100
125
cM

375

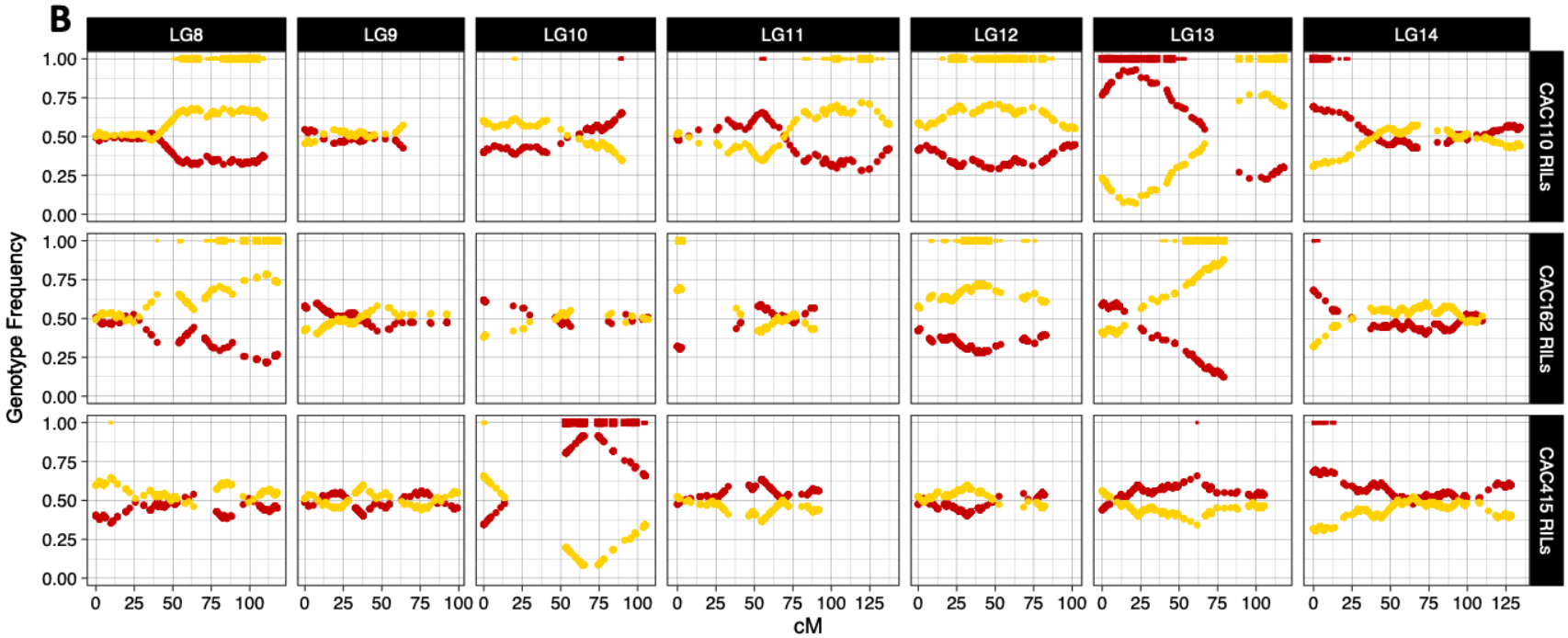

Figure 3. Transmission ratio distortion by map position, (a) Linkage group (LG) 1-7, (b) LG8-LG14. Genotype frequencies in windowed 50kb markers across the 14 linkage groups of the three RIL populations. Red dots indicate homozygous *M. guttatus* genotypes, yellow dots, homozygous *M. nasutus* genotypes. Bars at the top of each plot indicate regions showing significant transmission ratio distortion from the Mendelian 1:1 expectation by χ^2 tests at $\alpha = 0.01$ (thin bars), and a more stringent Bonferonni-corrected α (thick bars, unique α for each chromosome in each RIL population depending on the number of markers tested, see Table S3 for values). Bar color indicates an excess of *M. guttatus* (red), or *M. nasutus* (yellow) genotypes. Markers are ordered by genetic position within each map (cM).

384 notably, the proximal end of LG14 shows an excess of *M. guttatus* alleles in all three
385 populations. There is also an excess of *M. guttatus* alleles on LGs 1 and 4 and an excess of *M.*
386 *nasutus* alleles on LGs 8, 12, and 13 in two of the three RIL populations (CAC110 and CAC162).
387 These regions of shared distortion are largely confined to segments of the genome that are non-
388 introgressed in parental lines. In addition to local peaks of TRD among homozygous marker
389 genotypes, we also investigated levels of residual heterozygosity in the three RIL populations. At
390 the SNP level (RIL windowed genotypes exclude heterozygous calls; see Methods), we observed
391 low levels of heterozygosity (~1.5-3%) consistent with Mendelian expectations in F6/F7 RILs.
392 Residual heterozygosity was broadly uniform across the genome, with no clear regions enriched
393 for heterozygous SNP calls.
394
395 *Hybrid incompatibilities as a source of TRD*
396 In each RIL population, we identified several instances of two-locus epistasis (10 in the
397 CAC110 RILs, 4 in the CAC162 RILs, 9 in the CAC415 RILs: Table 2; Table S5). All but one of these
398 23 cases are due to a deficit of heterospecific allele combinations, consistent with the action of
399 hybrid incompatibilities reducing viability or fertility during RIL formation. In 16 of these cases,
400 the underlying mechanism seems to be epistatic selection favoring the same parental genotypes
401 – that is, we observed either an excess of *M. guttatus* genotypes or *M. nasutus* genotypes at
402 *both* loci. In six cases, however, there are clear deficits of only one of the two heterospecific
403 genotype combinations *and* the expected single-locus distortion stemming from selection
404 against the incompatible genotype at each locus (Table 2). This asymmetry is a hallmark of
405 Dobzhansky-Muller incompatibilities. In four of the six cases, loci involved in these

Table 2. Positions of two-locus epistasis. Physical (Mb) positions of pairs of loci on each linkage group (LG) in the three RIL populations that show LD (r) in the 95th percentile, as well as Chi-Square statistics from likelihood ratio tests with p<0.0001. Counts of each genotypic class in the population are shown. Loci marked with an asterisk have peak r and χ^2 values at adjacent markers. Single locus proportions of *M. guttatus* alleles (G Prop.) were used to determine if the pattern of TRD at each epistatic locus could be explained by a two-locus hybrid incompatibility (NG- or GN-), or if epistatic selection favoring the same parental genotypes better explains the pattern (GG or NN). The best candidates for two locus hybrid incompatibilities are shaded grey. See Table S5 for full list of epistatic loci in LD 95th percentile.

	Locus 1		Locus 2										Locus 1	Locus 2	
Population	LG	Mb	LG	Mb	r	GG	GN	NG	NN	N	χ2	p	G Prop.	G Prop.	Pattern
CAC110	03	20.40 - 22.65	13	3.05 - 5.20	0.56	64	3	17	19	103	32.552	<0.0001	0.65	0.79	GG
	05	3.10 - 20.75	11	2.55 - 4.90	0.54	39	21	1	22	83	29.035	<0.0001	0.72	0.48	NG-
	01	11.15 - 12.85	04	1.20 - 19.65	0.46	73	13	12	19	117	22.858	<0.0001	0.74	0.73	GG
	02	2.85 - 18.95	13	21.75 - 23.65	0.45	54	1	26	14	95	21.079	<0.0001	0.58	0.84	GG
	09	0.80 - 0.90	11	26.30 - 26.60	0.38	29	37	6	54	126	19.359	<0.0001	0.52	0.28	NG-
	05	2.40 - 20.90	11	5.05 - 10.20*	0.50	43	14	5	17	79	18.697	<0.0001	0.72	0.61	GG
	03	0.15 - 18.95	11	24.35 - 25.30	0.40	29	24	12	56	121	18.567	<0.0001	0.44	0.34	NN
	11	8.80 - 24.40	12	1.00 - 19.2	0.44	18	12	12	59	101	17.988	<0.0001	0.30	0.30	NN
	01	3.30 - 5.50	11	4.00 - 5.75	0.47	29	9	10	24	72	16.515	<0.0001	0.53	0.54	GG
	05	2.25 - 3.50	13	24.00 - 25.00	0.44	54	13	7	14	88	15.846	<0.0001	0.76	0.69	GG
CAC162	04	19.90 - 22.80	14	2.35 - 18.15	0.50	29	10	14	44	97	24.708	<0.0001	0.40	0.44	NN
	01	1.40 - 5.55	10	19.65 - 19.95	0.54	27	9	8	31	75	23.571	<0.0001	0.48	0.47	NN
	06	6.30 - 15.10	12	6.20 - 7.75	0.47	9	50	23	15	97	21.637	<0.0001	0.61	0.33	-
	01	2.35 - 5.45	03	0.00 - 20.65	0.45	28	21	7	42	98	20.628	<0.0001	0.50	0.36	NG-
CAC415	04	1.90 - 22.30	14	2.15 - 25.60	0.61	34	9	7	31	81	31.85	<0.0001	0.53	0.51	GG
	06	17.00 - 19.25	10	19.50 - 20.25	0.43	38	0	22	13	73	22.217	<0.0001	0.52	0.82	GG
	05	3.50 - 20.40	14	16.50 - 23.00	0.49	26	5	17	32	80	19.799	<0.0001	0.39	0.54	GN-
	07	13.20 - 21.80	08	22.30 - 27.70	0.48	23	7	14	38	82	19.719	<0.0001	0.37	0.45	NN
	13	22.05 - 25.55	14	0.00 - 3.00	0.47	41	6	15	20	82	18.738	<0.0001	0.57	0.68	GG
	06	9.65 - 16.00	08	23.60 - 25.55	0.44	22	10	12	37	81	15.892	<0.0001	0.40	0.42	NN
	01	5.85 - 7.40	04	4.10 - 16.55	0.43	32	6	18	24	80	15.338	<0.0001	0.48	0.63	GN-
	01	7.70 - 11.70	13	24.20 - 25.15	0.42	24	4	22	30	80	15.279	<0.0001	0.35	0.58	GN-
	05	20.85 - 21.75	06	7.10 - 16.05	0.43	20	11	11	40	82	15.242	<0.0001	0.38	0.38	NN

414 incompatibilities occur exclusively in non-introgressed regions. However, in two of the pairs, one
415 or both loci reside in introgressed blocks, suggesting there may also be segregating
416 incompatibilities within CAC *M. nasutus*. As with overall patterns of TRD, regions involved in
417 two-locus epistasis are largely population specific (although in some cases, we likely have
418 limited power to detect shared epistasis due to small sample sizes and genetic background
419 effects).
420
421 *Genetics of hybrid fertility traits*
422 Despite six generations of selfing, all three RIL populations exhibited substantial
423 variation in male fertility. Some of this variation may be due to inbreeding depression in *M.*
424 *guttatus* parental lines, which showed lower pollen viability than the *M. nasutus* parent (Figure
425 S14). However, heterospecific interactions are likely also involved, as all three RIL populations
426 include a considerable fraction of individuals (~10-22%) with pollen viability <50% (well below
427 the *M. guttatus* average of 72%; Figure S14). In the CAC110 RIL population, we mapped five
428 pollen viability QTLs accounting for ~36% of variance, including two separate epistatic pairs
429 (Table 3; Figure 4). One of these epistatic pairs leads to reduced male fertility in RILs with *M.*
430 *nasutus* alleles on LG4 and *M. guttatus* alleles on LG14 (Figure S15a). The pattern of TRD at
431 these same loci (excess of *M. guttatus* on LG4 and *M. nasutus* alleles on LG14; Figure 3) might
432 suggest the action of a gametic incompatibility that reduces pollen viability, but other genetic
433 mechanisms are also possible (e.g., a sporophytic incompatibility that reduces pollen viability to
434 the point of preventing effective self-fertilization/seed production). The second epistatic pair in
435 the CAC110 RIL population – between QTLs on LG12 and LG14 – also arises due to a negative

436 **Table 3. Male and female fertility QTL locations and effects in each mapping population.** Linkage group (LG), map (cM), and physical
437 (Mb) position of each significant QTL is shown. Additive effects (a) are negative when the *M. guttatus* allele has the lower value,
438 indicated in the summary column. QTLs with significant epistatic effects are shaded together. Percentage of RIL population variance
439 (PVE) is shown for each additive and epistatic effect. The 1.5-LOD interval of the QTLs underlying female fertility on LG10 in the
440 CAC415 RILs, marked with an asterisk, spans a breakpoint of the known derived inversion in the reference *M. guttatus* line IM62,
441 leading to a disjunct interval. Effect plots are shown in Figures S15-S18.

					Additive effect				Epistatic effect			
Population	Trait	LG	cM Position (1.5 LOD)	Mb Position (1.5 LOD)	a	PVE (%)	p	Summary	a x a	PVE (%)	p	Summary
CAC110 RILs	Male Fertility	4	26.975 (21.030 - 36.595)	16.70 - 16.75 (4.50 - 19.65)	-0.145	7.746	0.0008	G+	0.347	6.786	0.0004	NN+ (NG-)
		14	42.717 (37.467 - 48.317)	3.40 - 3.85 (3.05 - 4.30)	0.474	13.876	<0.0001	N+				
		11	132.951 (131.376 - 137.499)	26.65 - 26.70 (26.60 - 32.20)	-0.278	4.054	0.0059	G+				
		12	87.711 (80.538 - 101.548)	24.45 - 24.55 (23.25 - 25.80)	0.080	5.620	0.0055	N+	0.302	5.037	0.0022	NN+ (NG-)
		14	114.441 (112.343 - 116.889)	25.20 - 25.40 (25.00 - 25.60)	0.230	10.317	<0.0001	N+				
	Female Fertility	2	71.214 (62.399 - 86.970)	18.90 - 18.95 (18.40 - 20.55)	0.991	9.736	0.0001	N+				
		3	15.741 (11.890 - 20.758)	18.95 - 19.10 (18.40 - 19.95)	0.747	6.820	0.0012	N+				
		4	21.030 (16.833 - 26.101)	4.50 - 4.75 (3.85 - 16.70)	0.968	10.245	<0.0001	N+				
CAC162 RILs	Male Fertility	6	95.776 (90.673 - 95.776)	20.70 - 20.90 (19.25 - 20.90)	0.490	10.010	0.0011	N+				
		14	57.509 (54.192 - 61.594)	15.90 - 16.20 (7.05 - 16.80)	0.680	19.320	<0.0001	N+				
	Female Fertility	NA										
CAC415 RILs	Male Fertility	NA										
	Female Fertility	10	51.596 (48.660 - 53.554)	5.70 - 5.75 (4.50 - 5.75, 1.40 - 1.80)*	1.473	12.439	0.0022	N+				

442

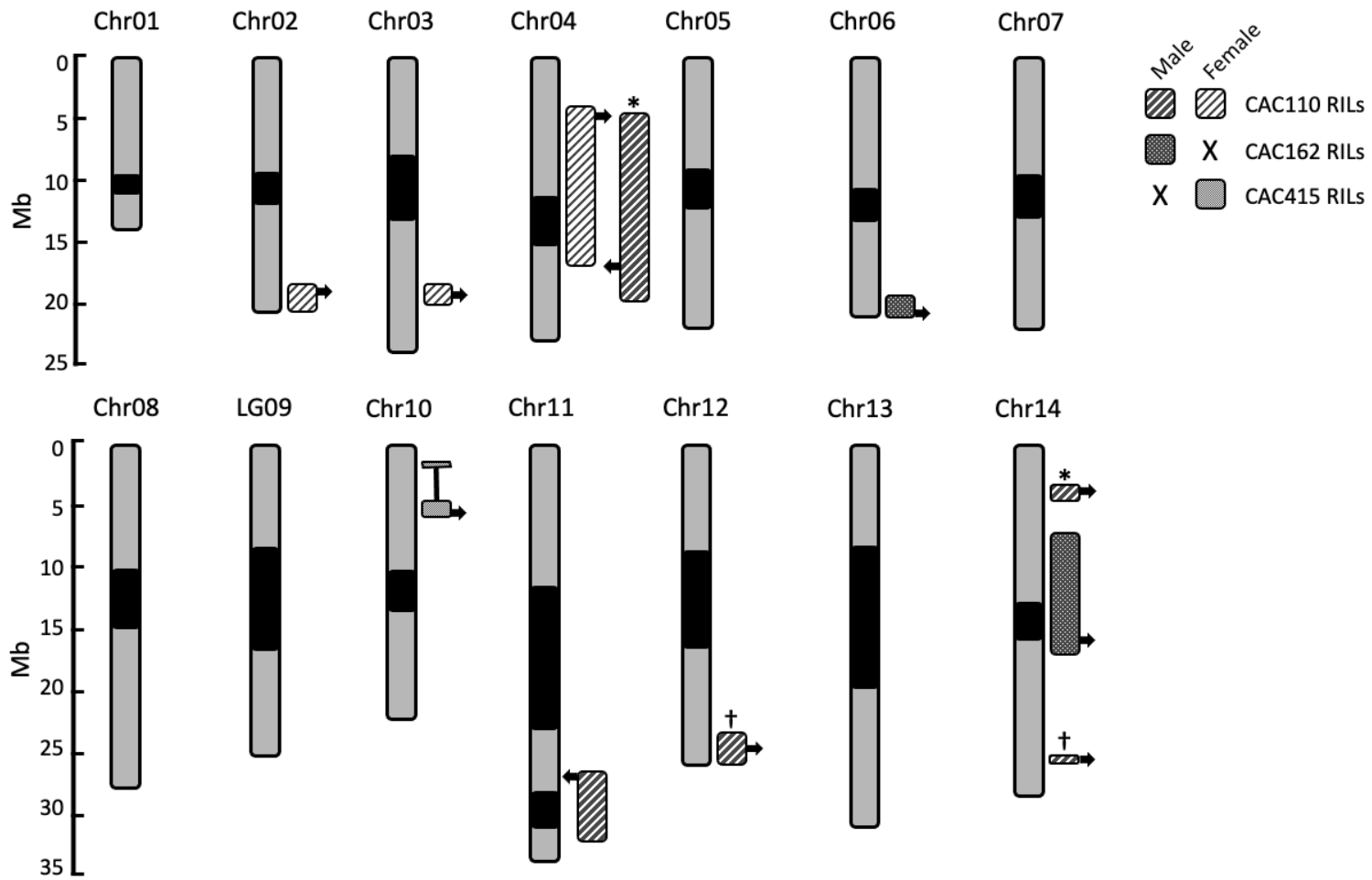

Figure 4. Male and female fertility QTL locations in each mapping population. Physical position (Mb) of the 1.5-LOD interval of each significant QTL is shown. Phenotype and RIL population indicated in key. Arrows indicate the position of peak marker(s). Arrows pointing left indicate the *M. guttatus* allele has the lower value, arrows pointing right indicate the *M. nasutus* allele has the lower value. QTLs with significant epistatic effects are indicated with shared symbols. The 1.5-LOD interval of the QTL underlying female fertility on Chr10 in the CAC415 RILs spans a breakpoint of the known derived inversion in the reference *M. guttatus* line IM62, leading to a disjunct interval. Centromere locations are indicated in black.

450 heterospecific interaction (RILs homozygous for *M. nasutus* alleles on LG12 and *M. guttatus* on
451 LG14 have the lowest fertility; Figure S15c), although *M. nasutus* genotypes have higher pollen
452 fertility at each QTL individually (Table 3). At the remaining QTL for male fertility on LG11, *M.*
453 *nasutus* alleles result in lower pollen viabilities (opposite to parental values), suggesting there
454 could be additional unmapped loci that interact with this QTL to decrease male fertility. In the
455 CAC162 RIL population, we mapped two QTLs for pollen viability (accounting for ~28% of the
456 variance), but because we detected no epistasis between them and *M. nasutus* alleles increased
457 fertility at both, these effects might be due to inbreeding depression or to incompatibilities with
458 additional loci below our detection thresholds. We mapped no QTLs for male fertility in the
459 CAC415 RIL population.

460 For female fertility, all three *M. guttatus* parents had much lower fruit production than
461 the *M. nasutus* parent, suggesting substantial inbreeding depression affecting this trait (Figure
462 S14). Accordingly, all QTLs we identified – three in the CAC110 RIL and one in the CAC415 RIL –
463 were additive with *M. nasutus* alleles increasing fertility (Table 3).

464 **Discussion**

465 Closely related species living in secondary sympatry, especially those displaying
466 incomplete reproductive isolation and still experiencing gene flow, provide an opportunity to
467 investigate the evolution and maintenance of reproductive barriers in nature. Here we construct
468 three RIL populations in one such system: hybridizing sister species *Mimulus guttatus* and *M.*
469 *nasutus* from the sympatric site Catherine Creek. Our multi-parent crossing design allows for a
470 uniquely powerful assessment of postzygotic barriers in a naturally admixed and highly
471 genetically diverse population. Overall, patterns of TRD and long-range LD, along with
472 interacting QTLs for hybrid sterility, provide evidence of multiple segregating hybrid
473 incompatibilities between these naturally hybridizing species. Additionally, these RILs are now a
474 permanent resource to be used in research on adaptation and speciation in *Mimulus*, facilitating
475 future experiments to identify the genes involved in hybrid incompatibilities and understand
476 their ecological context across environmental conditions.

477

478 *Introgression in sympatry: M. nasutus ancestry in CAC M. guttatus*

479 Consistent with previous work showing signatures of ongoing and historical
480 introgression at Catherine Creek (Brandvain *et al.*, 2014; Kenney & Sweigart, 2016), we
481 identified many clear tracks of admixture from *M. nasutus* across the genomes of the *M.*
482 *guttatus* parental lines (despite having chosen these lines for their species-diagnostic traits).
483 Despite pervasive admixture, these studies also showed a genome-wide, negative correlation
484 between recombination rate and divergence between species at Catherine Creek (Brandvain *et*
485 *al.*, 2014; Kenney & Sweigart, 2016). This same negative correlation has been discovered in

486 several other systems (Begun & Aquadro, 1993; Takahashi *et al.*, 2004; Keinan & Reich, 2010)
487 and is evidence that, in general, natural selection acts against *M. nasutus* ancestry in *M.*
488 *guttatus* genetic backgrounds. Consistent with this idea, many regions of introgression in the
489 three *M. guttatus* are unique to a single line. Despite this general pattern, two regions of
490 introgression, at the ends of chromosomes 3 and 4, are present in all three *M. guttatus* lines.
491 These same two regions also show elevated levels of gene flow (relative to the genome-wide
492 average) in wild admixed individuals at CAC (Figure 4, Kenney & Sweigart, 2016) suggesting they
493 might carry loci that are universally adaptive (Suarez-Gonzalez *et al.*, 2018) or that spread
494 through selfish processes (Lindholm & Price, 2016).

495 A key question at Catherine Creek is whether introgression is continuously renewed
496 through recent hybridization or instead reflects the remnants of past events. Nearly one-quarter
497 of the CAC110 genome shows evidence of *M. nasutus* ancestry, the expectation for a second-
498 generation (backcross) hybrid. Although this line does contain large genomic regions with
499 primarily *M. nasutus* ancestry (Figure S4), the largest actual block of introgression detected by
500 the HMM is only ~1.1 Mb, much smaller than what is expected in an early hybrid. In some
501 cases, there might be technical reasons for these breaks in introgression – genotyping errors, for
502 instance, or underestimates by the HMM (see Brandvain *et al.*, 2014, Text S1). However, we
503 note that use of variants in these regions largely improves the RIL genetic maps, indicating that
504 the breaks might often have biological causes. For example, crosses between hybrid individuals
505 might combine previously independent admixture events into larger, nearly contiguous blocks.
506 At Catherine Creek, we find evidence of a stable admixed population in certain microsites over a
507 period of more than 10 years (Farnitano et al., unpublished results), suggesting such mating

508 events might be quite frequent. Additionally, some of these apparent breaks in introgression
509 could be due to variation in *M. nasutus*, which has an average nucleotide diversity of ~1%
510 (Brandvain et al. 2014). Although most of this *M. nasutus* genetic variation is likely segregating
511 between rather than within populations (Sweigart & Willis, 2003), the long history of
512 introgression at Catherine Creek (Brandvain *et al.*, 2014; Kenney & Sweigart, 2016) might inflate
513 diversity between contemporary and remnants of past CAC *M. nasutus* samples (the latter
514 contained in introgressions). Finally, although introgression at Catherine Creek is highly
515 asymmetric, interspecific gene flow does occasionally go in the opposite direction, introducing
516 *M. guttatus* alleles into *M. nasutus* (Brandvain *et al.*, 2014). Such variation in *M. nasutus* could
517 also contribute to small blocks of *M. guttatus* ancestry identified within larger blocks of
518 introgression.
519
520 *M. nasutus as a source of structural variation in sympatric M. guttatus*
521 From this small sample of only three *M. guttatus* lines, we identified three previously
522 unknown structural variants segregating within *M. guttatus* at CAC, two of which appear to have
523 been introduced into *M. guttatus* from *M. nasutus.* Unlike reciprocal translocations, which can
524 cause F1 fertility problems through direct impacts on chromosomal segregation (Stathos &
525 Fishman, 2014; Sotola *et al.*, 2023), inversions often do not directly induce underdominant
526 hybrid sterility in plants (Fishman & Sweigart, 2018; Huang & Rieseberg, 2020; Zhang *et al.*,
527 2021). Nevertheless, loci for reproductive isolation have often been shown to map to inversions
528 (Noor *et al.*, 2001a,b; Livingstone & Rieseberg, 2004; Huang & Rieseberg, 2020; Todesco *et al.*,
529 2020), potentially because, in species still connected by some degree of gene flow, they prevent

530 selection from purging incompatibilities (Noor et al. 2001b) or lock together multiple linked
531 variants involved in divergent adaptation (Rieseberg et al. 2001, Kirkpatrick & Barton 2006).
532 Although none of the hybrid sterility QTLs we discovered map to any of the three inversions,
533 several putative incompatibilities do (Table 2, Figure S6), suggesting structural variation might
534 play a role in maintaining postzygotic isolation at Catherine Creek. Going forward, it will also be
535 important to determine whether traits involved in divergent ecological adaptation between CAC
536 *M. nasutus* and *M. guttatus* (Mantel & Sweigart, 2019) map to any of these inversions as has
537 been shown in ecotypes of *M. guttatus* (Lowry & Willis 2010) and sunflowers (Todesco et al.
538 2020).
539 Whatever their functional and fitness effects may be, the three inversions are likely to
540 have a large impact on patterns of admixture at Catherine Creek. In the most admixed of the
541 three *M. guttatus* parents (CAC110), roughly one-quarter of the introgression is within the
542 boundaries of the *inv1.2* and *inv13* inversions (Figure S2, Figure S6). An open question is
543 whether inverted regions display elevated levels of divergence as expected if they
544 disproportionately contribute to reproductive isolation and adaptive divergence (Noor et al.
545 2001, Rieseberg et al. 2001). If so, taking these regions into account might actually strengthen
546 the previously discovered negative relationship between absolute divergence and local
547 recombination (Brandvain *et al.*, 2014; Kenney & Sweigart, 2016), which relied on estimates of
548 recombination from genetic maps between non-CAC accessions.
549
550 *Variation in transmission ratio distortion and postzygotic isolation across experimental hybrid*
551 *populations*

552 Previous comparisons of TRD in *Mimulus* crosses between a common *M. guttatus* parent
553 (the annual line IM62) and either an allopatric *M. nasutus* line (SF) or a perennial *M. guttatus*
554 line (DUN) showed strong, but largely non-overlapping patterns of TRD (Hall & Willis 2005). In
555 this study, too, we find that patterns of TRD are highly variable across the three RIL populations,
556 although differences here can be attributed only to diversity within CAC *M. guttatus*. It is well
557 known that individual populations of *M. guttatus* contain a tremendous amount of genetic
558 variation (Flagel *et al.*, 2014; Puzey *et al.*, 2017) often with important phenotypic effects (Willis,
559 1992; Mojica *et al.*, 2012; Monnahan & Kelly, 2017). This study suggests this variation might
560 also have profound effects on reproductive barriers between species.
561 Although TRD may arise through several mechanisms (Fishman & McIntosh 2019), only
562 some of them are expected to produce the polymorphism we observe among RIL populations. A
563 consistent signal of TRD is expected in regions affected by purifying selection against weakly
564 deleterious *M. nasutus* alleles (i.e., hybridization load: Moran *et al.*, 2021) or by environmental
565 selection favoring *M. nasutus* alleles at loci responsive to the greenhouse growth conditions. On
566 the other hand, environmental selection favoring *M. guttatus* alleles (including epistatic
567 selection – see Table 2) will produce a consistent signal only if all three CAC *M. guttatus* parents
568 share the same functional alleles at causal loci. Similarly, inbreeding depression in *M. guttatus*
569 might be expected to produce variable patterns of TRD given that it is often caused by rare
570 deleterious alleles (Willis, 1999a,b). Because meiotic drivers are generally expected to fix rapidly
571 in the absence of associated fitness costs (Burt & Trivers, 1998), they might seem unlikely to
572 contribute to variable TRD. However, one such well-characterized driver – the centromeric *D*
573 allele in *M. guttatus* – is polymorphic in the Iron Mountain population where it was discovered,

574 and linked to alleles that reduce ferility (Fishman & Saunders, 2008). Thus, even selfish
575 segregation distorters might contribute to the variable patterns of TRD we observe in the CAC
576 RILs.

577 Another well-known cause of distortion – and the one with the most relevance for
578 speciation – is the reduced viability of gametes or zygotes due to hybrid incompatibilities
579 (Leppälä *et al.*, 2013; Kerwin & Sweigart, 2017). During RIL construction, gametic
580 incompatibilities may be particularly likely to persist, as even RILs with fewer viable ovules or
581 pollen grains can be successfully self-fertilized. Gametic incompatibilities affecting male and
582 female fertility have been identified in crosses between *M. guttatus* and *M. nasutus* (Kerwin &
583 Sweigart 2017) and between *M. parishii* and *M. cardinalis* (Sotola *et al.*, 2023), and the
584 genotypic ratios observed at many putative two-locus incompatibilities at CAC (Table 2) are
585 consistent with this mechanism of action. On the other hand, given that QTLs associated with
586 reductions in pollen viability (Table 3) do not map to distorted regions, it seems likely that these
587 incompatibilities disrupt male fertility in the diploid sporophyte. Whatever their mechanism, a
588 key point for this study is that hybrid incompatibilities between closely related species are often
589 polymorphic (López-Fernández & Bolnick, 2007; Cutter, 2012; Corbett-Detig *et al.*, 2013;
590 Charron *et al.*, 2014; Servedio & Hermisson, 2020). Moreover, in *Mimulus*, hybrid
591 incompatibility loci often vary *within* populations (Christie & Macnair, 1987; Sweigart *et al.*,
592 2007; Sweigart & Flagel, 2015; Zuellig & Sweigart, 2018a). In one case of duplicate genes that
593 cause hybrid seedling inviability between sympatric *M. guttatus* and *M. nasutus* at Don Pedro
594 Reservoir (DPR) in California (Zuellig & Sweigart, 2018b), at least some of the polymorphism
595 seems to be due to introgression from *M. nasutus* into *M. guttatus* (Zuellig & Sweigart, 2018a).

596 Given the large amount of admixture observed in CAC *M. guttatus*, it seems highly probable
597 that, like at DPR, interspecific gene flow contributes to polymorphism in hybrid incompatibilities
598 at Catherine Creek.

599 Despite this general variability, there is one region at the end of chromosome 14
600 consistently distorted in all three RIL populations (with an excess of *M. guttatus* alleles), which
601 may point to a conserved mechanism. This same region actually showed the opposite pattern of
602 distortion (an excess of *M. nasutus* alleles) in F_2 hybrids between IM62 *M. guttatus* and SF *M.*
603 *nasutus* (Fishman *et al.*, 2001, 2008), suggesting the underlying mechanism is not shared
604 species-wide and might be unique to CAC.

605

606 *Conclusions*

607 Overall, these RIL populations provide evidence of diverse contributors to postzygotic
608 isolation between *Mimulus* species, suggesting long-term persistence of hybrids at Catherine
609 Creek may be unlikely. Even highly admixed *M. guttatus* individuals carry alleles at multiple loci
610 that are incompatible with *M. nasutus*. This substantial load of hybrid incompatibilities may help
611 explain the observed cline of *M. nasutus* introgression in wild admixed individuals at Catherine
612 Creek (Kenney & Sweigart, 2016), which seems to suggest persistent backcrossing to *M.*
613 *guttatus* and purging of *M. nasutus* ancestry. Moreover, our findings of genome-wide TRD and
614 several retained fertility QTLs in the RILs supports previous evidence for broad, genome-wide
615 selection against *M. nasutus* ancestry in an *M. guttatus* background (Brandvain *et al.*, 2014;
616 Kenney & Sweigart, 2016). Thus, despite a long history of admixture at Catherine Creek,

617 intrinsic barriers between *Mimulus* species remain pervasive, limiting the homogenizing effects

618 of gene flow and, potentially, playing a key role in the maintenance of species.

619 **Author Contributions**

620 Research conceived and designed by SJM and ALS. Data collected and analyzed by SJM.
621 Manuscript written by SJM and ALS.

622

623 **Data Accessibility**

624 All whole genome sequence data of inbred lines and RADseq data of RILs will be
625 deposited at the NCBI Sequence Read Archive upon acceptance. Other data and scripts will be
626 made available from the Dryad Digital Repository.

627

628 **Acknowledgements**

629 We thank Amanda Kenney for seed collection at Catherine Creek. We are also grateful to
630 Aaliyah Stoudemire, Violet Iyahne, Suni Thakur, Brennen Anderson, and Selma Kajtazovic for
631 assistance with RIL creation, and Michaela Yarbough, Inam Jameel, and Mohamed Elgallad for
632 help with RIL crossing and fertility phenotyping. We thank greenhouse staff, Greg Cousins, Kevin
633 Tanner, Noah Hentherinton, and Mike Boyd for plant care. Jill Anderson, Lisa Donovan, Bob
634 Schmitz, and Mike White provided helpful discussions and guidance. Makenzie Whitener, Matt
635 Farnitano, and Natalie Gonzalez provided valuable comments on a previous draft. This work was
636 supported by a National Science Foundation grant [IOS-1827645 to ALS]; [DEB-1856223 to ALS];
637 funds from the University of Georgia Research Foundation [to ALS]; the National Institute of
638 General Medical Sciences of the National Institute of Health [T32GM007103 to SJM]; and the
639 UGA Genetics Jan and Kirby Alton Graduate Fellowship [to SJM].

640

641 **Competing Interests**

642 The authors declare no conflicts of interest.

643

644 **ORCID**

645 *Samuel J. Mantel* https://orcid.org/0000-0001-6392-4022

References

Ali OA, O'Rourke SM, Amish SJ, Meek MH, Luikart G, Jeffres C, Miller MR. **2016**. RAD Capture (Rapture): Flexible and Efficient Sequence-Based Genotyping. *Genetics* **202**: 389–400.

Arends D, Prins P, Jansen RC, Broman KW. **2010**. R/qtl: high-throughput multiple QTL mapping. *Bioinformatics* **26**: 2990–2992.

Aylor DL, Valdar W, Foulds-Mathes W, Buus RJ, Verdugo RA, Baric RS, Ferris MT, Frelinger JA, Heise M, Frieman MB, *et al.* 2011. Genetic analysis of complex traits in the emerging Collaborative Cross. *Genome Research* **21**: 1213–1222.

Barker WR, Nesom GL, Beardsley PM, Fraga NS. **2012**. A taxonomic conspectus of Phrymaceae: A narrowed circumscription for Mimulus, new and resurrected genera, and new names and combinations. *Phytoneuron* **2012–39**: 1–60.

Begun DJ, Aquadro CF. **1993**. African and North American populations of Drosophila melanogaster are very different at the DNA level. *Nature* **365**: 548–550.

Brandvain Y, Kenney AM, Flagel L, Coop G, Sweigart AL. **2014**. Speciation and Introgression between Mimulus nasutus and Mimulus guttatus. *PLOS Genetics* **10**: e1004410.

Broman KW, Sen S. **2009**. *A Guide to QTL Mapping with R/qtl*. New York, NY: Springer New York.

Burt A, Trivers R. **1998**. Selfish DNA and breeding system in flowering plants. *Proceedings of the Royal Society of London. Series B: Biological Sciences* **265**: 141–146.

Caeiro-Dias G, Brelsford A, Meneses-Ribeiro M, Crochet P-A, Pinho C. **2023**. Hybridization in late stages of speciation: Strong but incomplete genome-wide reproductive isolation and 'large Z-effect' in a moving hybrid zone. *Molecular Ecology* **32**: 4362–4380.

Charron G, Leducq J-B, Landry CR. **2014**. Chromosomal variation segregates within incipient species and correlates with reproductive isolation. *Molecular Ecology* **23**: 4362–4372.

Christie P, Macnair MR. **1987**. THE DISTRIBUTION OF POSTMATING REPRODUCTIVE ISOLATING GENES IN POPULATIONS OF THE YELLOW MONKEY FLOWER, MIMULUS GUTTATUS. *Evolution* **41**: 571–578.

Colomé-Tatché M, Johannes F. **2016**. Signatures of Dobzhansky–Muller Incompatibilities in the Genomes of Recombinant Inbred Lines. *Genetics* **202**: 825–841.

Corbett-Detig RB, Zhou J, Clark AG, Hartl DL, Ayroles JF. **2013**. Genetic incompatibilities are widespread within species. *Nature* **504**: 135–137.

Coyne JA, Orr HA. **2004**. *Speciation*. Oxford, New York: Oxford University Press.

Cutter AD. **2012**. The polymorphic prelude to Bateson–Dobzhansky–Muller incompatibilities. *Trends in Ecology & Evolution* **27**: 209–218.

Darwin C. **1859**. *On the Origin of Species*.

Delmore KE, Hübner S, Kane NC, Schuster R, Andrew RL, Câmara F, Guigó R, Irwin DE. **2015**. Genomic analysis of a migratory divide reveals candidate genes for migration and implicates selective sweeps in generating islands of differentiation. *Molecular Ecology* **24**: 1873–1888.

Dobzhansky T. **1937**. *Genetics and the Origin of Species*. New York, NY: Columbia University Press.

Durbin R, Eddy SR, Krogh A, Mitchison G. **1998**. *Biological Sequence Analysis: Probabilistic Models of Proteins and Nucleic Acids*. Cambridge: Cambridge University Press.

Ellegren H, Smeds L, Burri R, Olason PI, Backström N, Kawakami T, Künstner A, Mäkinen H, Nadachowska-Brzyska K, Qvarnström A, *et al.* 2012. The genomic landscape of species divergence in Ficedula flycatchers. *Nature* **491**: 756–760.

Feder JL, Roethele JB, Filchak K, Niedbalski J, Romero-Severson J. **2003**. Evidence for Inversion Polymorphism Related to Sympatric Host Race Formation in the Apple Maggot Fly, Rhagoletis pomonella. *Genetics* **163**: 939–953.

Fishman L, Aagaard J, Tuthill JC. **2008**. TOWARD THE EVOLUTIONARY GENOMICS OF GAMETOPHYTIC DIVERGENCE: PATTERNS OF TRANSMISSION RATIO DISTORTION IN MONKEYFLOWER (MIMULUS) HYBRIDS REVEAL A COMPLEX GENETIC BASIS FOR CONSPECIFIC POLLEN PRECEDENCE. *Evolution* **62**: 2958–2970.

Fishman L, Kelly AJ, Morgan E, Willis JH. **2001**. A Genetic Map in the Mimulus guttatus Species Complex Reveals Transmission Ratio Distortion due to Heterospecific Interactions. : 16.

Fishman L, McIntosh M. **2019**. Standard Deviations: The Biological Bases of Transmission Ratio Distortion. *Annual Review of Genetics* **53**: 347–372.

Fishman L, Sweigart AL. **2018**. When Two Rights Make a Wrong: The Evolutionary Genetics of Plant Hybrid Incompatibilities. *Annual Review of Plant Biology* **69**: 707–731.

Fishman L, Sweigart AL, Kenney AM, Campbell S. **2014a**. Major quantitative trait loci control divergence in critical photoperiod for flowering between selfing and outcrossing species of monkeyflower (Mimulus). *The New Phytologist* **201**: 1498–1507.

Fishman L, Willis JH, Wu CA, Lee Y-W. **2014b**. Comparative linkage maps suggest that fission, not polyploidy, underlies near-doubling of chromosome number within monkeyflowers (Mimulus; Phrymaceae). *Heredity* **112**: 562–568.

Flagel LE, Blackman BK, Fishman L, Monnahan PJ, Sweigart A, Kelly JK. **2019**. GOOGA: A platform to synthesize mapping experiments and identify genomic structural diversity. *PLOS Computational Biology* **15**: e1006949.

Flagel LE, Willis JH, Vision TJ. **2014**. The Standing Pool of Genomic Structural Variation in a Natural Population of Mimulus guttatus. *Genome Biology and Evolution* **6**: 53–64.

Good JM, Handel MA, Nachman MW. **2008**. ASYMMETRY AND POLYMORPHISM OF HYBRID MALE STERILITY DURING THE EARLY STAGES OF SPECIATION IN HOUSE MICE. *Evolution* **62**: 50–65.

Hoffmann AA, Rieseberg LH. **2008**. Revisiting the Impact of Inversions in Evolution: From Population Genetic Markers to Drivers of Adaptive Shifts and Speciation? *Annual Review of Ecology, Evolution, and Systematics* **39**: 21–42.

Huang K, Rieseberg LH. **2020**. Frequency, Origins, and Evolutionary Role of Chromosomal Inversions in Plants. *Frontiers in Plant Science* **11**.

Jansen RC, Stam P. **1994**. High resolution of quantitative traits into multiple loci via interval mapping. *Genetics* **136**: 1447–1455.

Jones FC, Grabherr MG, Chan YF, Russell P, Mauceli E, Johnson J, Swofford R, Pirun M, Zody MC, White S, *et al.* 2012. The genomic basis of adaptive evolution in threespine sticklebacks. *Nature* **484**: 55–61.

Kearns C, Inouye D. **1993**. *Techniques for Pollination Biologists*. Niwot, CO: University of Colorado Press.

Keinan A, Reich D. **2010**. Human Population Differentiation Is Strongly Correlated with Local Recombination Rate. *PLOS Genetics* **6**: e1000886.

Kenney AM, Sweigart AL. **2016**. Reproductive isolation and introgression between sympatric Mimulus species. *Molecular Ecology* **25**: 2499–2517.

Kerwin RE, Sweigart AL. **2017**. Mechanisms of Transmission Ratio Distortion at Hybrid Sterility Loci Within and Between Mimulus Species. *G3 Genes|Genomes|Genetics* **7**: 3719–3730.

Larson EL, White TA, Ross CL, Harrison RG. **2014**. Gene flow and the maintenance of species boundaries. *Molecular Ecology* **23**: 1668–1678.

Leppälä J, Bokma F, Savolainen O. **2013**. Investigating Incipient Speciation in Arabidopsis lyrata from Patterns of Transmission Ratio Distortion. *Genetics* **194**: 697–708.

Lindholm AK Guest Editors, Price TAR. **2016**. The evolutionary consequences of selfish genetic elements. *Current Zoology* **62**: 655–658.

Livingstone K, Rieseberg L. **2004**. Chromosomal evolution and speciation: a recombination-based approach. *New Phytologist* **161**: 107–112.

Long AD, Macdonald SJ, King EG. **2014**. Dissecting complex traits using the Drosophila Synthetic Population Resource. *Trends in Genetics* **30**: 488–495.

López-Fernández H, Bolnick DI. **2007**. What Causes Partial F1 Hybrid Viability? Incomplete Penetrance versus Genetic Variation. *PLOS ONE* **2**: e1294.

Lowry DB, Sobel JM, Angert AL, Ashman T-L, Baker RL, Blackman BK, Brandvain Y, Byers KJRP, Cooley AM, Coughlan JM, *et al.* 2019. The case for the continued use of the genus name Mimulus for all monkeyflowers. *TAXON* **68**: 617–623.

Lowry DB, Willis JH. **2010**. A Widespread Chromosomal Inversion Polymorphism Contributes to a Major Life-History Transition, Local Adaptation, and Reproductive Isolation. *PLOS Biology* **8**: e1000500.

Mantel SJ, Sweigart AL. **2019**. Divergence in drought-response traits between sympatric species of Mimulus. *Ecology and Evolution* **9**: 10291–10304.

Martin NH, Willis JH. **2007**. Ecological Divergence Associated with Mating System Causes Nearly Complete Reproductive Isolation between Sympatric Mimulus Species. *Evolution* **61**: 68–82.

Mayr E. **1942**. *Systematics And The Origin Of Species*.

Mojica JP, Lee YW, Willis JH, Kelly JK. **2012**. Spatially and temporally varying selection on intrapopulation quantitative trait loci for a life history trade-off in Mimulus guttatus. *Molecular Ecology* **21**: 3718–3728.

Monnahan PJ, Kelly JK. **2015**. Naturally segregating loci exhibit epistasis for fitness. *Biology Letters* **11**: 20150498.

Monnahan PJ, Kelly JK. **2017**. The Genomic Architecture of Flowering Time Varies Across Space and Time in Mimulus guttatus. *Genetics* **206**: 1621–1635.

Moran BM, Payne C, Langdon Q, Powell DL, Brandvain Y, Schumer M. **2021**. The genomic consequences of hybridization (PJ Wittkopp, Ed.). *eLife* **10**: e69016.

Moyle LC, Nakazato T. **2008**. Comparative Genetics of Hybrid Incompatibility: Sterility in Two Solanum Species Crosses. *Genetics* **179**: 1437–1453.

Nesom GL, Fraga NS, Barker WR, Beardsley PM, Tank DC, Baldwin BG, Olmstead RG. **2019**. Response to “The case for the continued use of the genus name Mimulus for all monkeyflowers”. *TAXON* **68**: 624–627.

Nolte AW, Gompert Z, Buerkle CA. **2009**. Variable patterns of introgression in two sculpin hybrid zones suggest that genomic isolation differs among populations. *Molecular Ecology* **18**: 2615–2627.

Noor MAF, Grams KL, Bertucci LA, Almendarez Y, Reiland J, Smith KR. **2001a**. The Genetics of Reproductive Isolation and the Potential for Gene Exchange between Drosophila pseudoobscura and D. persimilis via Backcross Hybrid Males. *Evolution* **55**: 512–521.

Noor MAF, Grams KL, Bertucci LA, Reiland J. **2001b**. Chromosomal inversions and the reproductive isolation of species. *Proceedings of the National Academy of Sciences* **98**: 12084–12088.

Paradis E. **2010**. pegas: an R package for population genetics with an integrated–modular approach. *Bioinformatics* **26**: 419–420.

Puzey JR, Willis JH, Kelly JK. **2017**. Population structure and local selection yield high genomic variation in Mimulus guttatus. *Molecular Ecology* **26**: 519–535.

Rastas P. **2017**. Lep-MAP3: robust linkage mapping even for low-coverage whole genome sequencing data. *Bioinformatics* **33**: 3726–3732.

Renaut S, Grassa CJ, Yeaman S, Moyers BT, Lai Z, Kane NC, Bowers JE, Burke JM, Rieseberg LH. **2013**. Genomic islands of divergence are not affected by geography of speciation in sunflowers. *Nature Communications* **4**: 1827.

Scott MF, Ladejobi O, Amer S, Bentley AR, Biernaskie J, Boden SA, Clark M, Dell'Acqua M, Dixon LE, Filippi CV, *et al.* 2020. Multi-parent populations in crops: a toolbox integrating genomics and genetic mapping with breeding. *Heredity* **125**: 396–416.

Servedio MR, Hermisson J. **2020**. The evolution of partial reproductive isolation as an adaptive optimum. *Evolution* **74**: 4–14.

Servedio MR, Kirkpatrick M. **1997**. The Effects of Gene Flow on Reinforcement. *Evolution* **51**: 1764–1772.

Sotola VA, Berg CS, Samuli M, Chen H, Mantel SJ, Beardsley PA, Yuan Y-W, Sweigart AL, Fishman L. **2023**. Genomic mechanisms and consequences of diverse postzygotic barriers between monkeyflower species. : 2023.04.21.537885.

Stathos A, Fishman L. **2014**. Chromosomal rearrangements directly cause underdominant F1 pollen sterility in Mimulus lewisii–Mimulus cardinalis hybrids. *Evolution* **68**: 3109–3119.

Sweigart AL, Flagel LE. **2015**. Evidence of Natural Selection Acting on a Polymorphic Hybrid Incompatibility Locus in Mimulus. *Genetics* **199**: 543–554.

Sweigart AL, Mason AR, Willis JH. **2007**. NATURAL VARIATION FOR A HYBRID INCOMPATIBILITY BETWEEN TWO SPECIES OF MIMULUS. *Evolution* **61**: 141–151.

Sweigart AL, Willis JH. **2003**. Patterns of Nucleotide Diversity in Two Species of Mimulus Are Affected by Mating System and Asymmetric Introgression. *Evolution* **57**: 2490–2506.

Takahashi A, Liu Y-H, Saitou N. **2004**. Genetic Variation Versus Recombination Rate in a Structured Population of Mice. *Molecular Biology and Evolution* **21**: 404–409.

Taylor EB, Boughman JW, Groenenboom M, Sniatynski M, Schluter D, Gow JL. **2006**. Speciation in reverse: morphological and genetic evidence of the collapse of a three-spined stickleback (Gasterosteus aculeatus) species pair. *Molecular Ecology* **15**: 343–355.

Teeter KC, Thibodeau LM, Gompert Z, Buerkle CA, Nachman MW, Tucker PK. **2010**. The Variable Genomic Architecture of Isolation Between Hybridizing Species of House Mice. *Evolution* **64**: 472–485.

Todesco M, Owens GL, Bercovich N, Légaré J-S, Soudi S, Burge DO, Huang K, Ostevik KL, Drummond EBM, Imerovski I, *et al.* 2020. Massive haplotypes underlie ecotypic differentiation in sunflowers. *Nature*: 1–6.

Willis JH. **1992**. Genetic analysis of inbreeding depression caused by chlorophyll-deficient lethals in Mimulus guttatus. *Heredity* **69**: 562–572.

Willis JH. **1999a**. The contribution of male-sterility mutations to inbreeding depression in Mimulus guttatus. *Heredity* **83**: 337–346.

Willis JH. **1999b**. Inbreeding Load, Average Dominance and the Mutation Rate for Mildly Deleterious Alleles in Mimulus guttatus. *Genetics* **153**: 1885–1898.

Yu J, Holland JB, McMullen MD, Buckler ES. **2008**. Genetic Design and Statistical Power of Nested Association Mapping in Maize. *Genetics* **178**: 539–551.

Zeng ZB. **1993**. Theoretical basis for separation of multiple linked gene effects in mapping quantitative trait loci. *Proceedings of the National Academy of Sciences* **90**: 10972–10976.

Zeng ZB. **1994**. Precision mapping of quantitative trait loci. *Genetics* **136**: 1457–1468.

Zhang L, Reifová R, Halenková Z, Gompert Z. **2021**. How Important Are Structural Variants for Speciation? *Genes* **12**: 1084.

Zuellig MP, Sweigart AL. **2018a**. A two-locus hybrid incompatibility is widespread, polymorphic, and active in natural populations of Mimulus*. *Evolution* **72**: 2394–2405.

Zuellig MP, Sweigart AL. **2018b**. Gene duplicates cause hybrid lethality between sympatric species of Mimulus. *PLOS Genetics* **14**: e1007130.

836